Available online at www.sciencedirect.com
ScienceDirect
Journal of the European Ceramic Society 31 (2011) 1481–1490
www.elsevier.com/locate/jeurceramsoc

Ceramic foams and micro-beads from emulsions of a preceramic polymer

Cekdar Vakifahmetoglu [1], Marco Balliana, Paolo Colombo *

Dipartimento di Ingegneria Meccanica, Settore Materiali, University of Padova, 35131 Padova, Italy

Received 26 November 2010; received in revised form 27 January 2011; accepted 6 February 2011
Available online 26 February 2011

Abstract

A commercially available solid silicone resin was dissolved in a solvent and emulsified via stirring in the presence of water and surfactant to form three different types of emulsions, namely water-in-oil (w/o), water-in-oil-in-water (w/o/w) and oil-in-water (o/w), by following different preparation procedures. After curing, thermosets possessing different morphologies, ranging from highly porous (monolithic) foams to porous micro-beads and solid micro-beads, formed. The samples kept their shape upon pyrolysis, and resulted in ceramic foams (via w/o) and porous micron sized (∼200 μm) spherical particles (via w/o/w) having more than 80 vol% of total porosity, while with o/w emulsification solid SiOC ceramic particles with an average diameter of ∼100 μm formed. Both surfactant and water altered the IR spectra for emulsion-derived thermoset samples, in comparison to the pure cured resin, but upon pyrolysis similar amorphous ceramics were obtained from all samples.

Keywords: Preceramic polymers; Porous ceramics; Emulsion; Microbeads

1. Introduction

Preceramic polymers have been under intensive research, due to their attractive properties (such as commercial availability, easy handling, versatile shaping capability, and low temperature processing) starting from early 1960s. In addition, they are suitable candidates for the manufacture of advanced ceramics at significantly lower temperatures ($T < 1500\,^{\circ}C$) than conventional powder sintering processing. These polymeric precursors are organic–inorganic polymers with a backbone usually containing Si atoms, and through the elimination of organic moieties give ceramic residues termed polymer derived ceramics (PDCs).[1] Fibers, coatings, porous media, or complex-shaped bulk parts have been produced by using preceramic polymers.[2] In particular, highly porous silicon oxycarbide (SiOC) and silicon carbonitride (SiCN) ceramics were obtained using polysiloxane and polysilazane precursors, respectively, through several processing strategies.[3–8] Among these methods, emulsion processing of preceramic polymers to produce ceramic components has so far received relatively little attention.[9–13] Recently, this approach was applied to the fabrication of SiOC ceramics with different shapes, e.g. porous components (max porosity < 52% and <40% by using polycarbosilane and polysiloxane precursors, respectively) or solid micro-beads.[12,13] While open celled ceramic foams have never been manufactured by emulsion processing, Ye et al.[14] demonstrated a robust microfluidic technique generating monodispersed single and double emulsion drops to form solid and porous SiOC ceramic micron sized (generally <200 μm in diameter) particles and capsules from polysiloxanes by using microcapillary devices. An alternative method for the production of porous spheroidal ceramic beads is also electro-spraying of preceramic polymers, as demonstrated by Nangrejo et al.[15] In this paper, we present a more simple emulsion-based technique, not requiring any specialized equipment, to form SiOC ceramic bodies with various morphologies, ranging from highly porous (monolithic) open-celled foams to porous or solid micro-beads.

2. Experimental procedure

2.1. Materials

All experiments were performed using the following commercially available chemicals without further purification: a polymethylsilsesquioxane preceramic polymer (MK Bel-

* Corresponding author at: Department of Materials Science and Engineering, The Pennsylvania State University, University Park, PA 16802, USA.
E-mail addresses: cekdar@rci.rutgers.edu (C. Vakifahmetoglu), paolo.colombo@unipd.it (P. Colombo).
[1] Current address: Department of Materials Science and Engineering Rutgers, The State University of New Jersey, NJ 08854, USA.

0955-2219/$ – see front matter © 2011 Elsevier Ltd. All rights reserved.
doi:10.1016/j.jeurceramsoc.2011.02.012

sil, Wacker GmbH, Burghausen, Germany), denoted as PMS in the remainder of the text; zirconium acetylacetonate, $Zr[CH_3C(O)CHC(O)CH_3]_4$ (98%, Sigma–Aldrich, Munchen, Germany), added as a crosslinking agent for the silicone resin; toluene (ACS reagent ≥99.7%), as the oil phase; polyoxyethylene-sorbitan-20-monooleate (also known as polysorbate 80 or commercially as Tween 80, Sigma–Aldrich, St. Louis, MO), acting as a surfactant; and deionized (DI) water. From these chemicals, three different types of emulsions, namely water-in-oil (w/o), water-in-oil-in-water (w/o/w) and oil-in-water (o/w) were prepared, following different preparation procedures.

2.2. Preparation of highly porous monoliths via water-in-oil (w/o) emulsion

Porous monoliths were prepared via water in oil (w/o) emulsion. First, 5 g of silicone resin (PMS), as received in powder form, was dissolved in 7 mL toluene under magnetic stirring at room temperature (RT) for 15 min to produce a solution (oil phase). Such high solid containing solution can be obtained as a result of the excellent solubility of the PMS precursor in toluene.[13] In another beaker, the aqueous phase was prepared by adding 1 g of Tween 80 to 15 mL of DI water (surfactant was added very slowly), so that an aqueous solution possessing a much higher concentration of Tween 80 than that required for the critical micelle concentration (CMC ∼15 mg/L, in water at 20–25 °C)[16] was formed. When each solution became homogenous, the aqueous phase (DI water and surfactant) was added into oil phase (5 g PMS in 7 mL toluene) in a drop-wise manner while the mixture was stirred with a magnetic stirrer at 500 rpm. After addition of aqueous phase was completed, zirconium acetylacetonate (3 wt% with respect to the PMS mass, 0.15 g) was added as cross-linking agent (henceforth referred as CLA), and the blend was stirred for further 15 min at RT. The silicone resin contains hydroxyl and ethoxy groups which can react and cross-link.[17] The liquid mixture contained in a Pyrex beaker was then inserted into an oven and the temperature was increased to 140 °C with 5 °C/min heating rate. No lid was positioned on the beaker and following holding time of 12 h at this temperature in air, porous thermoset bodies formed.

2.3. Preparation of highly porous micro-beads via water-in-oil-in-water (w/o/w) emulsion

In order to prepare w/o/w emulsions, first a primary water-in-oil emulsion was prepared by following the steps described in Section 2.2, using the same chemicals but with 20 mL of DI water phase including 0.25 g of Tween 80 surfactant (into oil phase: 5 g PMS in 7 mL toluene). After stirring the primary emulsion for 30 min (500 rpm), a w/o/w emulsion was formed by dispersing at RT the w/o emulsion with an additional 60 mL of the aqueous phase (including 0.75 g of surfactant) while mixing with a magnetic stirrer (500 rpm). Upon completing the addition of the aqueous phase, CLA was added to the liquid and the produced double emulsion was further mixed at RT for 10 min until the w/o/w emulsion thickened. The heat treatment to cross-link the preceramic polymer was conducted in the same way as described in Section 2.2.

2.4. Preparation of solid micro-beads via oil-in-water (o/w) emulsion

Solid spherical micro-beads were formed via oil-in-water (o/w) emulsion in which the oil phase (5 g PMS in 7 mL toluene) was added at RT into an aqueous phase (80 mL DI water with 1 g of surfactant) in a drop-wise manner, while the blend was mixed by a magnetic stirrer at 500 rpm. Upon completing the addition of the oil phase addition, CLA was added and the formed emulsion was further mixed for 15 min (500 rpm) at RT. The mixture was then crosslinked in an oven in the same way described in Section 2.2.

2.5. Characterization

All of the cured samples were subsequently pyrolyzed at 1200 °C for 2 h with a 2 °C/min heating/cooling rate under N_2 atmosphere. The true density was measured from finely ground (ball milled at 300 rpm for 24 h) ceramic powder using a He-Pycnometer (Micromeritics AccuPyc 1330, Norcross, GA). Open porosity of the sintered ceramics was determined by mercury intrusion porosimetry (MIP, Porosimeter 2000, Carlo Erba Instruments, Milano, Italy). Fresh emulsions were analyzed by a stereo-microscope (type 376788, Wild Heerbrugg, Switzerland) and photomicrographs were captured by a digital camera (Coolpix 990, Nikon, Tokyo, Japan) mounted on the stereo-microscope. The morphological features of the emulsion structures (both cured and pyrolyzed bodies) were analyzed from fresh fracture surfaces using a scanning electron microscope (SEM, JSM-6300F, JEOL, Tokyo, Japan). SEM images were subsequently analyzed with the ImageTool software (UTHSCSA, University of Texas, USA) to quantify the cell and particle size and size distribution. The data obtained by image analysis were converted to 3D values to obtain the effective cell dimension by applying the stereological equation: $D_{sphere} = D_{circle}/0.785$.[18] X-ray diffraction data (XRD, Bruker D8-Advance, Karlsruhe, Germany) were collected using Cu $K_{\alpha 1}$ radiation (40 kV, 40 mA, step scan of 0.05°, counting time of 3 s/step). Raman spectra were recorded with an Invia Raman microspectrometer (Renishaw plc., Gloucestershire, U.K.) attached to a confocal microscope (50× objective) using the 633 nm line of an He–Ne laser as the excitation wavelength. Samples were ground and the powders were used for analysis, using a low laser power (5%). Infrared absorption spectra were recorded by Fourier transform infrared spectroscopy (FTIR) (Jasco 620 Spectrometer, Essex, UK), in the range 4500–400 cm^{-1} from an average of 50 scans on each sample, with a resolution of 2 cm^{-1}. Dried powders (ceramic or thermoset) were ground and mixed with potassium bromide (KBr) in 1:100 ratio by weight, and then pressed into a pellet form for FTIR test. The crushing strength (average of 5 indi-

vidual tests) of the porous monoliths was measured at room temperature by compression test, using (Instron 5569 UTM, Norwood, MA, USA; cross-head speed of 0.5 mm/min), on samples of nominal size ~5 mm × 5 mm × 5 mm, cut from larger specimens.

3. Results and discussion

All the emulsified mixtures throughout the study were first analyzed by optical stereo-microscopy and the results are given in the each section. For this aim, some drops of the formed emulsion were taken from the beaker and placed on a clear glass slide and then immediately analyzed by a stereo-microscope. It was observed that the morphologies obtained through the emulsifying stage remained practically unchanged after curing the preceramic polymer at 140 °C, which occurred with concurrent evaporation of toluene and water. It was already shown that the PMS precursor can be cured thermally in air at temperatures ~100 °C with the addition of CLA in less than 30 min.[17] Increased catalyst concentration enhances the rigidity of the material and decreases the temperature at which the cross-linking starts to occur. For example, with the addition of 2 wt% CLA, a viscoelastic behavior necessary for the cross-linking of PMS precursor could be reached at 105 °C.[17] Therefore, it is reasonable to assume that, in the present experimental conditions, the emulsified samples very rapidly (i.e. less than 15 min) reached a condition in which the polymer would not soften anymore, and the components were then able to maintain their shape.

The surfactant used in the formulations, Tween 80, is a non-ionic surfactant characterized by the presence of $CHO(CH_2CH_2O)nCH_2CH_2OH$ hydrophilic and $(CH_2)_7CH(C_8H_{18})CH_3$ hydrophobic parts.[19] It has a relatively high cloud point (65 °C) and an hydrophile–lipophile balance (HLB) value of ~15.[16] The cloud point is the temperature below which a single phase of molecular or micellar solution exists; above the cloud point the surfactant loses sufficient water solubility and a cloudy dispersion occurs. Above this temperature, the surfactant also ceases to perform some or all of its normal functions.[20] Under this perspective, Bakumov et al.[13] stated that, in order to use preceramic polymers and surfactants in emulsion processing, some requirements need to be met, in particular a high cloud temperature (>100 °C) of the selected surfactant. Our results, however, indicate that the functionality of the surfactant is a parameter of interest only before the preceramic polymer reaches a sufficient curing level; in fact, after an adequate viscoelasticity (degree of curing) is achieved, there is no more need for the action of the surfactant. Indeed, in the present system processed above the cloud temperature of Tween 80 surfactant, the emulsified mixtures had enough stability and so a partial or complete loss of amphiphilic properties was not detrimental (note that the amount of surfactant used in our experiments was also much higher than that of the minimum for CMC, and this might also affect the observed behavior. The clarification of this point, however, requires further experiments which are currently in progress).

3.1. Morphological characterization

3.1.1. Highly porous monoliths via water-in-oil (w/o) emulsion

Individual droplets surrounded by an "oil" phase can be clearly observed from the photomicrographs taken from the fresh emulsions formed when 15 mL (see Fig. 1(a) and (b)) of aqueous phase were added to the oil phase. The mean droplet (sphere) size, measured by image analysis tool using ~600 data points ($D_{sphere} = D_{circle}/0.785$), was 256 ± 201 μm. A large dispersion in the droplet size can be observed, which is expected since macro-emulsions are inherently unstable systems in which the initial droplets (typically >1 μm) may undergo coalescence. In order to reduce the scattering in droplet size, more stable emulsion systems such as mini- or micro-emulsions should be produced.[21]

The morphology of the cured and pyrolyzed sample prepared by adding 15 mL of aqueous phase is shown in Fig. 2(a and b) and (c and d), respectively. A well distributed, interconnected porosity is present within the material, exhibiting relatively small (50 ± 52 μm) cell windows, i.e. pores interconnecting adjacent cells, and large spherical cells in the order of ~200–400 μm which formed from the merging of individual water droplets during curing.[22] The morphology of the polymeric thermoset did not change significantly during pyrolysis, because of the high degree of cross-linking achieved during the curing step, and some volumetric shrinkage was observed but no cracks were found throughout the ceramic structure. The mean cell window size and cell size of the ceramic sample were 47 ± 37 μm and 173 ± 171 μm, respectively. The non homogeneous morphology of the porous body is therefore due to the large scattering in water droplet size values in the initial emulsion, together with the coalescence of the water droplets occurring during water and oil phase evaporation. The mechanism responsible for the formation of porosity is clearly linked to the evaporation of both entrapped water and solvent from the emulsified system. The release of volatiles (e.g. oligomers) from the preceramic polymer during curing and pyrolysis is another contributing factor to further increase the total amount of porosity in the ceramized bodies. It should be noted that the struts contained also a significant amount of voids (see strut detail given in Fig. 2(d), inset). This is because during cross-linking of the silicone resin with the help of CLA, the viscosity of the solution increased, leading to the conservation of the pores within the mass.

3.1.2. Highly porous micro-beads via water-in-oil-in-water (w/o/w) emulsion

Similarly to the previous experiments, the initial investigation was conducted on the as prepared emulsion by optical microscopy. A digital image showing the fresh emulsion prepared from 80 mL total aqueous phase is shown in Fig. 3(a, and inset therein). In this case, multiple emulsions where small water droplets are entrapped within polymeric (oil) droplets, which in turn are themselves dispersed in a continuous water phase (secondary), were obtained. The cured samples also were analyzed by optical microscopy, see Fig. 3

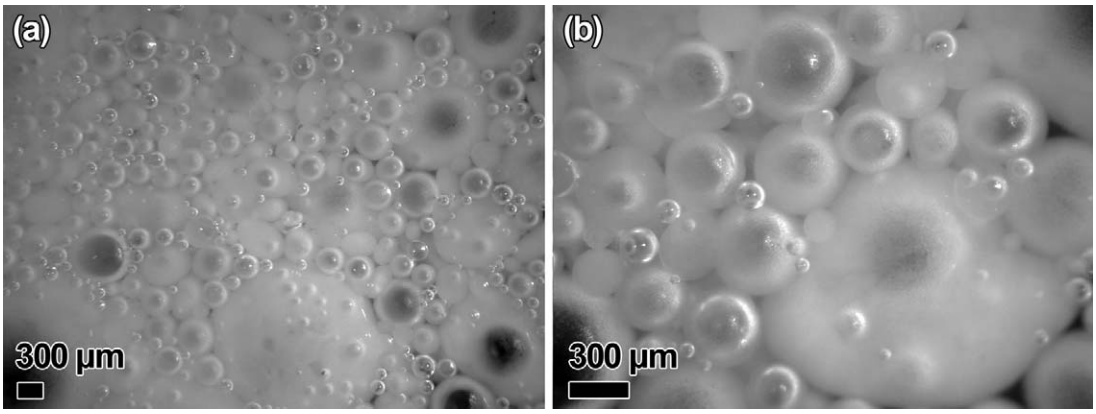

Fig. 1. Digital photos taken with a stereo-microscope from the emulsions (before curing) upon addition to the oil phase of 15 mL of aqueous phase; (a) general and (b) higher magnification view.

(b, and inset therein). Since during curing all the dispersing liquid media (water and toluene) disappeared, loosely packed spherical porous thermoset particles having mean particle size of 211 ± 84 μm were produced after the cross-linking step.

Cured samples were additionally examined by SEM. As it can be observed in Fig. 4(a) and (b), porous micro-beads were obtained upon curing of the mixture, possessing a mean particle size of 234 ± 86 μm. In Fig. 4(c) and (d), SEM images obtained from the fractured surfaces of pyrolyzed particles are shown. Ceramization enabled full retention of the morphology of the preceramic micro-beads, indicating again that the cross-linking procedure was appropriate to avoid (even partial) melting of the silicone polymer upon heating. The mean particle size and cell window size (interconnecting pores) were 190 ± 66 μm and 22 ± 10 μm, respectively. Bakumov et al.[12] showed that, depending on the shear forces introduced during the formation of the emulsions, the diameters of the ceramic beads can be controlled. They formed solid spherical particles with diameters of 1–10 μm and 10–100 μm when the emulsions were prepared with a homogenizer at stir rates up to 20,000 rpm or a magnetic stirrer at 1000 rpm, respectively.

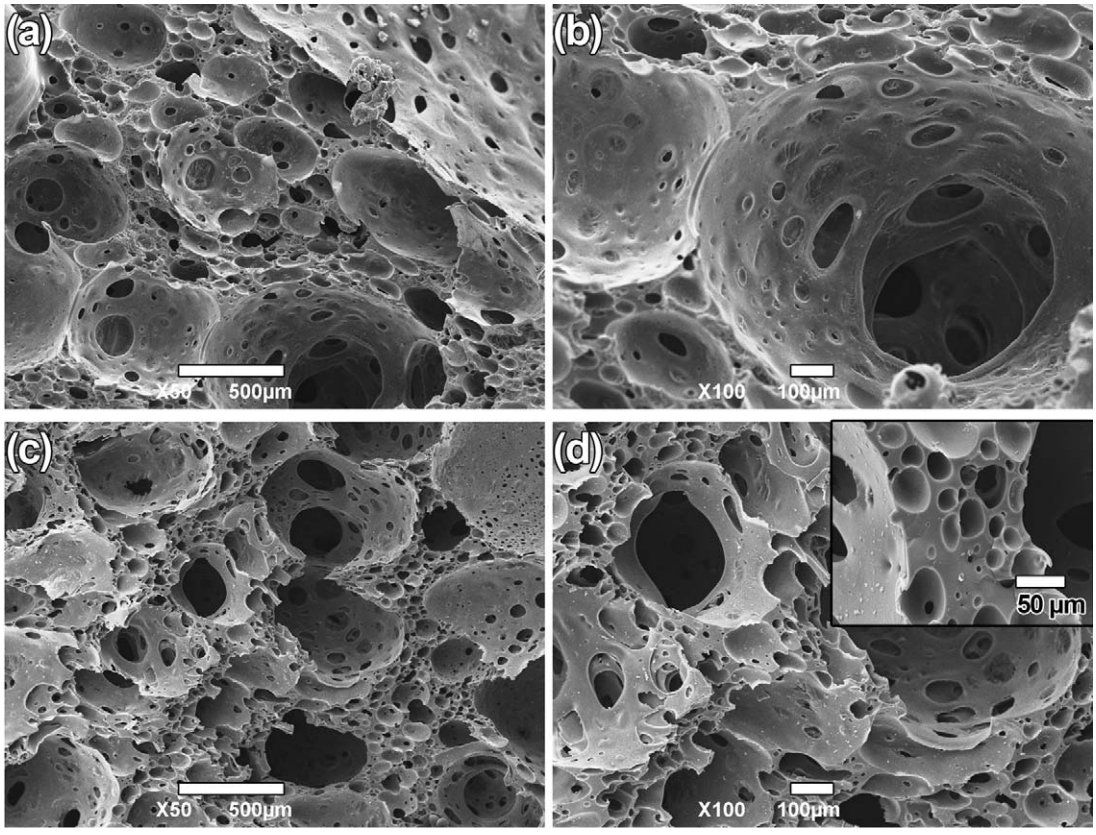

Fig. 2. SEM images of: (a) general morphology of cured porous thermoset; (b) higher magnification image; (c) general morphology of pyrolyzed component; and (d) higher magnification image (inset shows the detail of a strut).

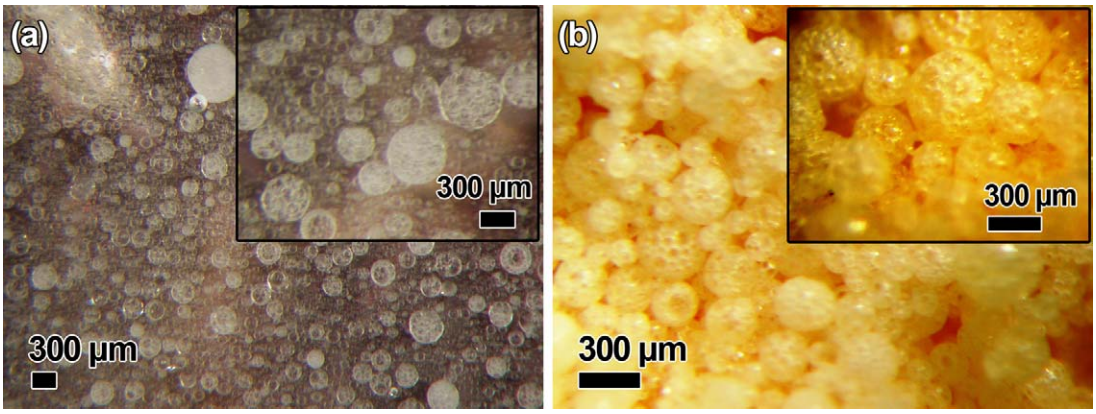

Fig. 3. Digital photos taken with a stereo-microscope of: (a) emulsions before curing upon 80 mL total aqueous phase addition, and (b) after curing (water and toluene evaporated), sample with 80 mL total aqueous phase. Insets report higher magnification images.

The solid particles with diameters > 10 μm obtained by those authors[12] had severe cracking problem, which was attributed to the well known generation of tensile stresses caused by the shrinkage and gas evolution occurring during the thermal decomposition of the crosslinked polymer. Instead, in the present system, the gaseous products could easily be released during pyrolysis at a slow heating rate, since the particles possessed and interconnected porous network, with no damage to the structure even for micro-beads of the largest diameter (>200 μm).

Some additional samples were prepared in order to examine the influence of the composition of the mixture (in particular the concentration of the preceramic polymer in the oil phase) on the development of the internal open porosity. Particles were formed, based again on a multiple emulsion, using half the amount of toluene to dissolve the PMS precursor, with respect to the original samples shown in Fig. 4(a–d). As seen in Fig. 4(e), the formed particles were bonded to each other by a silicone layer when they were in the polymeric state, and no open porosity was clearly visible at their surface. Rather, bigger particles or agglomerates formed (probably the shear rate was not adequate for such high viscous mixture), having an inner porosity which was mainly closed and inhomogeneous in size, as shown in Fig. 4(f) for a pyrolyzed sample. The results for a sample containing a double amount of toluene were different. The particle size was smaller, with large scattering in the diameter size, and possessing a porous outer layer. The images for this sample are not reported here for the sake of brevity. In the study by Bakumov,[13] in which they produced porous components from water-in-oil (w/o) emulsions, it was shown that the amount of solvent should be minimized in order not to avoid the formation of cracks during its evaporation upon cross-linking (note that the authors used an autoclave system to cure the emulsions), while our results demonstrate that when a w/o/w emulsion is formed, and curing is conducted in open air, the amount of solvent in the oil phase should rather be sufficient enough to obtain both well dispersed micro-beads (via the reduction of the viscosity of the oil phase) and the formation of interconnected porosity. Of course, further experiments should be conducted to determine the precise compositional boundaries which affect the morphology of the beads.

3.1.3. Solid micro-beads via oil-in-water (o/w) emulsion

Fig. 5(a) and inset show that non porous spherical thermoset beads were formed via an oil-in-water emulsion. These micro-beads were pyrolyzed, and SEM investigations (Fig. 5(b)) showed that the mean particle size was 111 ± 46 μm. Most particles appear to be connected by a thin ridge, creating a network of solid particles with interparticle porosity. Analysis of freshly fractured surfaces (see Fig. 5(c) and (d)) demonstrates that no cracks and no internal porosity can be observed, albeit the presence of pores with a diameter smaller than 1–2 μm should not be excluded (see later). While we obtained slightly larger micro-beads than that of the study by Bakumov et al.[12], no cracks associated to pyrolysis were observed in the present work. The difference could be simply the heating rate that was used in these studies: while we used 2 °C/min as the heating rate, Bakumov et al. used a rate of 40 °C/min.[12]

3.2. Characterization of the porosity and mechanical properties

The bulk density (ρ_b) is defined as the mass to volume (including the volume of both open and closed porosity, and of solid skeleton) ratio and it can be estimated by mercury porosimetry when the head pressure is at sub-atmospheric low values (3.5 kPa). Apparent density (sometimes termed apparent skeletal density), on the other hand, includes only the closed porosity, and can be found when all the open pores are filled with mercury at the highest pressure point. Consequently, from the mercury porosimetry data, one can easily calculate the open porosity. On the other hand, the true density (the density of the solid material without open or closed porosity, ρ_{true}), is defined as the ratio of mass to solid volume (with no porosity) and can be estimated by gas (helium) pycnometer when testing very fine powders (i.e. assuming of no closed porosity is still present). The total porosity was, therefore, calculated by combining the data for

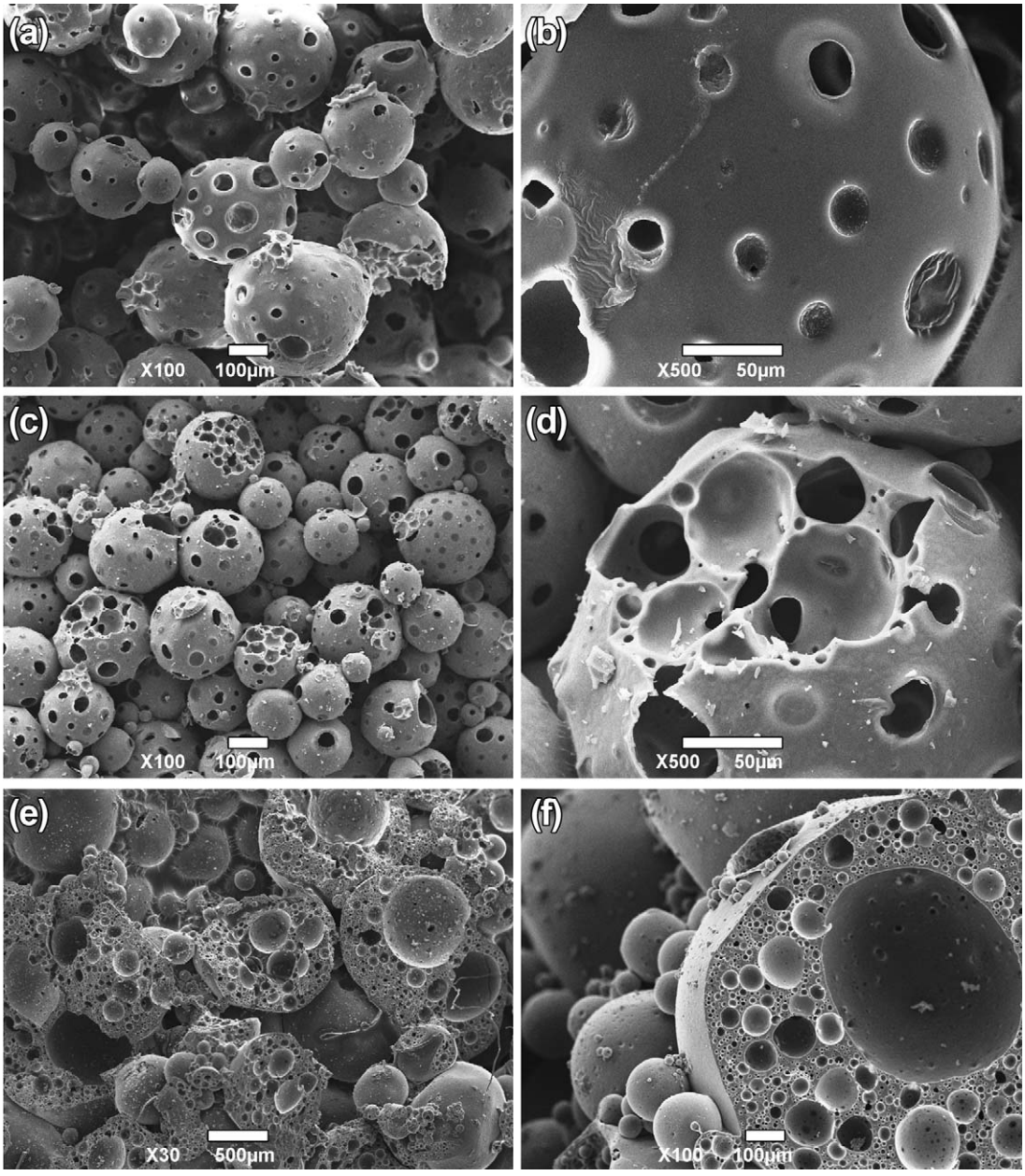

Fig. 4. SEM images taken from the sample prepared by using 80 mL aqueous phase; (a) general morphology of the cured micro-beads, (b) high magnification image, (c) general morphology of the pyrolyzed micro-beads, (d) high magnification image showing interconnected porosity in the particles, (e) general morphology of the cured polymer prepared by using half of the amount of toluene to dissolve the PMS precursor, and (f) pyrolyzed sample showing the inhomogeneous and mainly closed porosity within the particles.

the bulk density (obtained from mercury porosimetry measurements) and the true density (obtained from helium pycnometry measurements) in the following equation:

$$\text{Total porosity} = 100 \times \left(1 - \left(\frac{\rho_b}{\rho_{true}}\right)\right)$$

Data reported in Table 1 show that the porous monoliths and porous micro-beads had very high total porosity, being 89 vol% (68 vol% open pores) and 83 vol% (64 vol% open pores), respectively. It should be noted that the skeletal density values of these samples were still lower than the true density of SiOC found by helium pycnometer (which was 2.284 g/cm^3, after ball milling the pyrolyzed samples for 24 h), confirming that the cell walls or struts in the samples contained closed porosity, as already shown by SEM investigations (see Fig. 2(d, inset) and Fig. 4(d)). The pore diameter (up to 200 μm) distribution versus relative pore volume (%) curves obtained from Hg-porosimetry is given in Fig. 6(a–c). It seems that, while both the porous monolith and porous micro-beads had a broad pore size distribution, the curves possess two separate peaks located around 12–14 μm and 20–40 μm, 6–8 μm and 40–60 μm, respectively. For these samples, the pore formation was governed by the evaporation of water (entrapped in the polymeric network) and solvent from the emulsified system; the release of volatile species contained

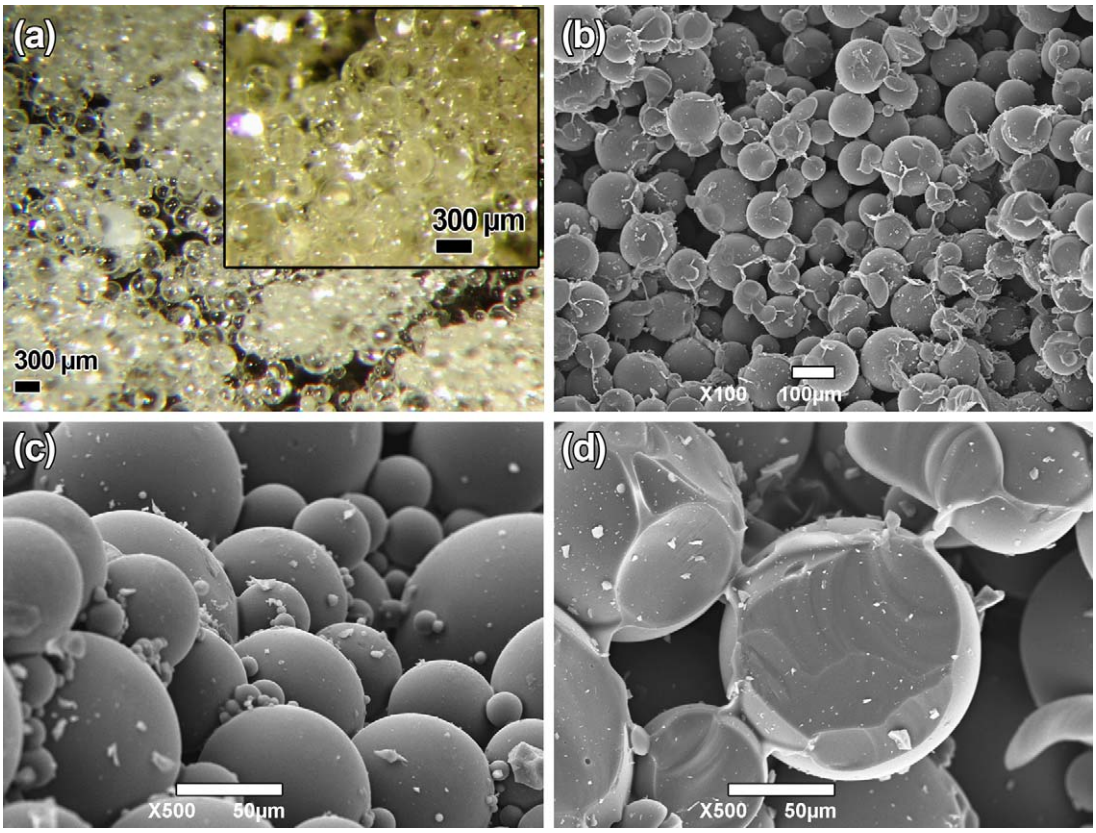

Fig. 5. (a) Stereo-microscopy image of cured o/w emulsion (inset shows higher magnification); SEM images of pyrolyzed micro-beads: (b) general morphology, (c) higher magnification image of the beads, and (d) high magnification image of fractured micro-particles showing that no porosity was present inside the micro-beads.

Table 1
Data from Hg intrusion, helium pycnometry and crushing tests.

	Porous monolith	Porous micro-beads	Solid micro-beads
Total cumulative volume (mm^3/g)	2825.81	1606.25	296.07
Total surface area (m^2/g)	12.71	4.88	2.20
Bulk density (g/cm^3) at 0.51 psia	0.241	0.398	0.962
Skeletal density (g/cm^3)	0.751	1.103	1.345
Average pore diameter (4V/A) (µm)	38.64	68.00	54.58
Open porosity (vol%)	68.0	63.9	28.5
Total porosity, calculated according to bulk density (vol%)[a]	89.5	82.6	57.9
Compression strength (MPa)	0.43 ± 0.13	n.a.	n.a.

[a] True density of the samples was 2.284 g/cm^3 (as measured by helium pycnometry).

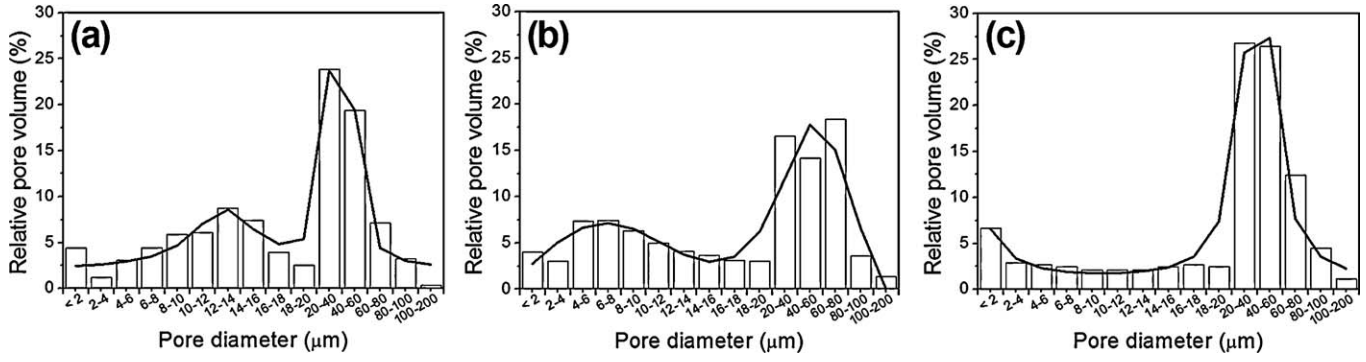

Fig. 6. Pore size (diameter) distribution versus relative pore volume (%) curves obtained from Hg-porosimetry of the pyrolyzed samples; (a) porous monolith (via w/o emulsion), (b) porous micro-beads (via w/o/w emulsion), and (c) solid micro-beads (via o/w emulsion).

in the preceramic polymer during both curing and pyrolysis also contributed to the increase in porosity.

The mercury porosimetry data obtained from the solid particles revealed unexpectedly high amount of total porosity 57.9 vol% (29.4 vol% closed and 28.5 vol% open porosity). It is clear from the pore diameter plot (in Fig. 6(c)) that this sample includes bi-modal pore size distribution having pores below ~2 μm (with a higher portion of pore volume compared to other samples) and above ~20 μm in diameter. With reference to the SEM images shown in Fig. 5(b–d), together with the data reported in Table 1 and Fig. 6(c), we can state that the high total porosity value measured in this sample is related mainly to the interparticle voids (both plugged (i.e. not through) pores and interconnected pores, generally with diameter > 20 μm, see Fig. 5(b) and (d)) formed due to residual thin ridge in between the beads forming a network-like structure, while pores below <1–2 μm might be associated with the transient porosity which was not eliminated during pyrolysis. This, in fact, could also be a contributing factor to why no cracks were observed in the pyrolyzed solid particles.

The average compressive strength of the monolithic foam sample, which possessed the highest total porosity of 89.5 vol% (68.0 vol% open pores), was 0.43 ± 0.13 MPa. The presence of porosity in the struts (see Fig. 2(d)) is the reason for the low strength values measured, in comparison to SiOC foams of similar relative density.[23] The presence of cells with a non homogeneous size distribution does not represent a particular problem, since several important properties are not linked to the cell size but rather simply to the relative density of the component.[24]

The present experiments demonstrate that it is possible to obtain monolithic macrocellular ceramics with mainly open porosity from emulsion processing of preceramic polymers. However, the decision of adopting this processing technique rather than competing alternatives, such as direct foaming, will depend on the best compromise possible among required properties, easy of processing and overall cost.

3.3. Structural characterization

FTIR spectra taken from the cured samples are reported in Fig. 7(left); for the sake of the comparison, spectra of pure PMS, PMS with CLA (both cured in the same conditions) and pure Tween 80 surfactant are also included in the graphs. In the spectra for PMS and PMS + CLA, the absorption of Si–CH_3 (1280–1255 cm^{-1}) bond located around 1275 cm^{-1}, which is assisted by deformation vibration band at around 770 cm^{-1} (asymmetric Si–CH_3), and also the vibration of SiOC–H around 2980 cm^{-1} and 550 cm^{-1} were clearly visible.[17] However, the intensity of those peaks was quite reduced in micro-beads (both porous and solid) deriving from emulsions. Apart from this difference, while PMS and PMS + CLA samples showed infrared spectra characterized by typical vibration bands at 1120 cm^{-1} (Si–O–Si) and 1030 cm^{-1} (Si–OR), for emulsified samples the intensity of the latter band decreased and left behind a broad band located around 1100 cm^{-1}, which can be assigned to both Si–O–Si (coming from PMS) and stretching of the C–O (coming from surfactant).[25] On the other hand, emulsified samples had additional peaks at around 1730 cm^{-1} belonging to C=O stretching band,[25] at 1630 cm^{-1} assigned to stretching of C=C,[25] at 1460 cm^{-1} and 1350 cm^{-1} attributed to C–H bending vibrations in $–CH_3$ and $–CH_2$, respectively,[25,26] a broad peak in between 3200 and 3650 cm^{-1} for O–H stretching band,[25,26] at 2925 cm^{-1} and 2860 cm^{-1} due to the asymmetrical and symmetrical C–H stretching of $–CH_2–$, respectively.[25] All of these additional peaks were more intense in micro-bead samples (both porous and solid) in comparison to highly porous monolith, certainly due to the strong adsorption of the surfactant on the surface of these micro-beads, as previously observed by other researchers.[25,27,28] Clearly, the major contribution in these spectra is that of the Tween 80 surfactant, and this might be the reason for the reduced spectral features related to the silicone resin itself.

The spectra of the same samples pyrolyzed at 1200 °C are shown in Fig. 7(right). All the pyrolyzed samples (both pure PMS and emulsified samples) had a broad peak centering ~1080 cm^{-1}, attributed to Si–O stretching vibration of Si–O–Si or Si–O–C units.[26] Deformation vibrations of Si–O–Si units can be seen from the peak ~450 cm^{-1}.[26] Another distinct band can be seen at ~800 cm^{-1} is due to the Si–C stretching vibrations.[14,26] While emulsion derived systems had different peaks than that of the non emulsified PMS systems in the polymeric state, after pyrolysis basically the same FTIR spectra were

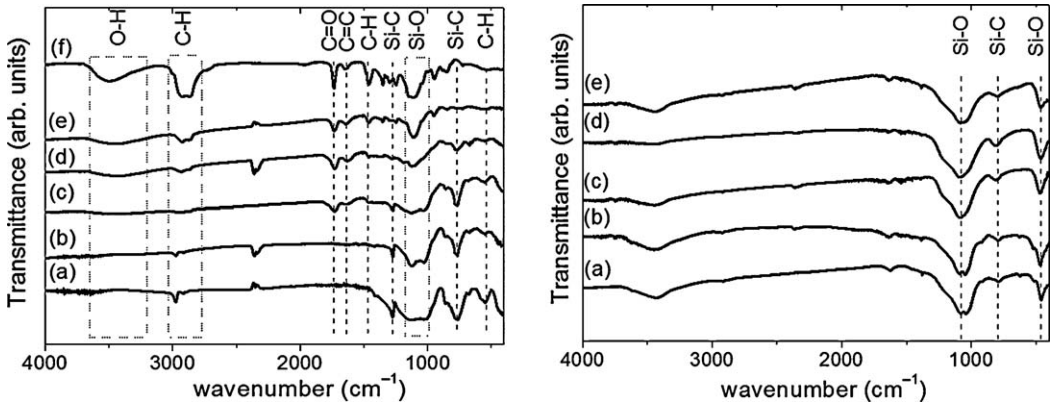

Fig. 7. FTIR spectra of the (left) cured and (right) pyrolyzed samples; (a) pure PMS precursor, (b) PMS + CLA, (c) porous monolith (via w/o emulsion), (d) porous micro-beads (via w/o/w emulsion), (e) solid micro-beads (via o/w emulsion), and (f) pure Tween 80.

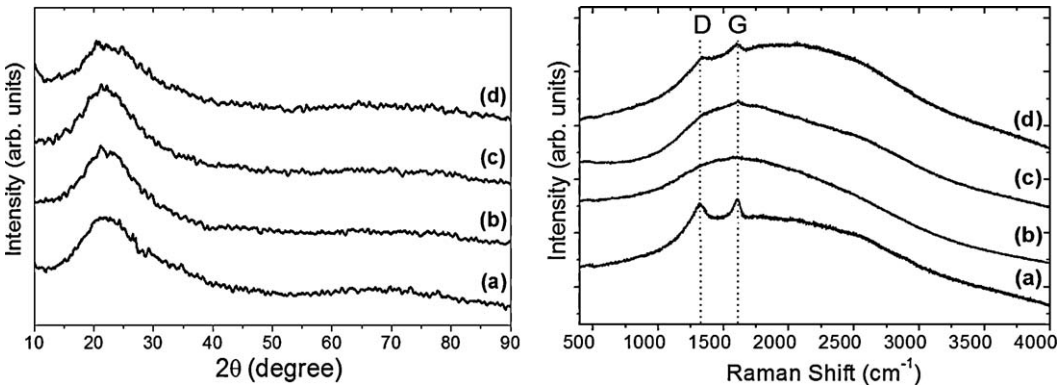

Fig. 8. XRD (left) and Raman (right) data for the pyrolyzed samples; (a) pure PMS precursor, (b) porous monolith (via w/o emulsion), (c) porous micro-beads (via w/o/w emulsion), and (d) solid micro-beads (via o/w emulsion).

obtained for all samples, indicating the formation of a SiOC ceramic material.

XRD analyses (see Fig. 8(left)) of the ceramic micro-beads showed the lack of crystalline phases in all the samples treated at this processing temperature, as only broad Bragg reflections between 10° and 30° range (2θ), attributable to an amorphous silicate-based material, is visible. Raman spectroscopy was applied to the pyrolyzed samples, see Fig. 8(right). All the sample had fluorescence background, which is a common phenomenon for PDCs produced at low temperatures ($\leq$1200 °C).[29] Pure PMS-derived SiOC and solid SiOC micro-beads (via o/w emulsion) showed two in-plane modes: the characteristic disorder-induced D-mode at $\sim$1320 cm^{-1} observed in carbon with finite crystallite size and the graphite G-mode near 1607 cm^{-1}, suggesting the presence of disordered graphitic carbon.[30,31] Evidently, the peaks in the spectra for solid micro-beads are less intense. Interestingly, these peaks are not clearly noticeable in the data obtained for the porous monolith (via w/o emulsion) and the porous micro-beads (via w/o/w emulsion).

It has been reported that the pronounced fluorescence phenomenon prevents the identification of the free carbon phase in SiOC ceramics formed by the pyrolysis up to 1400 °C.[29] Besides, it has been recently demonstrated that water (or water vapor) reduces the carbon in SiOC ceramics.[32] While, no Raman data were presented in that paper, it was shown, using solid state NMR spectroscopy, that the pyrolysis of polysiloxanes in the presence of water vapor remarkably modifies the atomic bonding configurations, and suppresses the precipitation of free-carbon in the pyrolyzed ceramic. It was proposed that the water-carbon reduction proceeds through the attacking by water of the carbon-containing organic groups, such as Si–CH_3/Si–CH_2–Si and Si–CH_3 (depletion of Si–C bonds), to form more Si–O bonds in the SiOC ceramic.[32] Although further detailed structural studies are needed, the lack of D and G peaks in the spectra for the porous monolith (via w/o emulsion) and porous micro-beads (via w/o/w emulsion), and the depression in the intensity of those peaks for the solid micro-beads (via o/w emulsion), might be simply associated with high fluorescence, making the bands no more distinguishable (defects and pores can also be effective in this regard).[29] However, it is also probable that water vapor suppresses the free carbon precipitation (especially in the w/o and w/o/w), making it drop fall below the monitoring threshold for those samples (note that the detection limit of Raman for carbon is $\geq$1 wt%). It should be noted that all the produced samples were anyway black, but it is known that even less than 0.2 wt% carbon may lead to a coloration of the glass.[33]

4. Conclusions

A simple, versatile method to produce various ceramic components from emulsion processing of a preceramic polymer is presented. Three different types of emulsions, namely water-in-oil (w/o), water-in-oil-in-water (w/o/w) and oil-in-water (o/w) were prepared, and after curing and pyrolysis, SiOC ceramic foam monoliths with a $\sim$89 vol% total porosity, porous micron sized spherical beads (average diameter 190 $\pm$ 66 μm) with a $\sim$83 vol% total porosity, and solid particles with a diameter of 111 $\pm$ 46 μm were produced. The ceramic foam possessed a low compression strength (0.43 $\pm$ 0.13 MPa), because of the porosity contained in the struts, but it can be considered to be adequate for their use in several engineering applications. A strong adsorption of the surfactant on the micro-beads surfaces together with water altered the IR spectra for thermoset samples, while upon pyrolysis similar amorphous ceramics formed from both pure and emulsified silicone resins.

Acknowledgements

The authors are greatly indebted to Prof. M. Meneghetti and Dr. V. Amendola of the University of Padova (Dipartimento di Scienze Chimiche) for the use of Micro-Raman equipment, and to Prof. G.D. Soraru and Dr. A. Karakuscu of the University of Trento (Dipartimento di Ingegneria dei Materiali e Tecnologie Industriali) for the use of Mercury porosimetry equipment.

References

1. Colombo P, Mera G, Riedel R, Soraru GD. Polymer-derived ceramics: 40 years of research and innovation in advanced ceramics. *J Am Ceram Soc* 2010;**93**:1805–37.
2. Colombo P, Soraru GD, Riedel R, Kleebe HJ, editors. *Polymer derived ceramics. From nano-structure to applications*. Lancaster, PA: DESTech Publications; 2009.

3. Colombo P. Engineering porosity in polymer-derived ceramics. *J Eur Ceram Soc* 2008;**28**:1389–95.
4. Vakifahmetoglu C, Colombo P. A direct method for the fabrication of macro-porous SiOC ceramics from preceramic polymers. *Adv Eng Mater* 2008;**10**:256–9.
5. Kumar BVM, Young-Wook K. Processing of polysiloxane-derived porous ceramics: a review. *Sci Technol Adv Mater* 2010;**11**:044303.
6. Vakifahmetoglu C, Menapace I, Hirsch A, Biasetto L, Hauser R, Riedel R, et al. Highly porous macro- and micro-cellular ceramics from a polysilazane precursor. *Ceram Int* 2009;**35**:3281–90.
7. Vakifahmetoglu C, Pauletti A, Fernandez Martin C, Babonneau F, Colombo P. SiOC ceramic monoliths with hierarchical porosity. *Int J Appl Ceram Technol* 2010;**7**:528–35.
8. Zeschky J, Höfner T, Arnold C, Weißmann R, Bahloul-Hourlier D, Scheffler M, et al. Polysilsesquioxane derived ceramic foams with gradient porosity. *Acta Mater* 2005;**53**:927–37.
9. Jones BH, Lodge TP. High-temperature nanoporous ceramic monolith prepared from a polymeric bicontinuous microemulsion template. *J Am Chem Soc* 2009;**131**:1676–7.
10. Otoishi S, Tange Y. Growth rate and morphology of silicon carbide whiskers from polycarbosilane. *J Cryst Growth* 1999;**200**: 467–71.
11. Kockrick E, Krawiec P, Petasch U, Martin H-P, Herrmann M, Kaskel S. Porous CeOX/SiC nanocomposites prepared from reverse polycarbosilane-based microemulsions. *Chem Mater* 2007;**20**: 77–83.
12. Bakumov V, Schwarz M, Kroke E. Emulsion processing and size control of polymer-derived spherical Si/C/O ceramic particles. *Soft Mater* 2006;**4**:287–99.
13. Bakumov V, Schwarz M, Kroke E. Emulsion processing of polymer-derived porous Si/C/(O) ceramic bodies. *J Eur Ceram Soc* 2009;**29**: 2857–65.
14. Ye C, Chen A, Colombo P, Martinez C. Ceramic microparticles and capsules via microfluidic processing of a preceramic polymer. *J R Soc Interface* 2010;**7**:461–73.
15. Nangrejo M, Bernardo E, Colombo P, Farook U, Ahmad Z, Stride E, et al. Electrohydrodynamic forming of porous ceramic capsules from a preceramic polymer. *Mater Lett* 2009;**63**:483–5.
16. Sigma–Aldrich. 'Detergent selection table: "Detergents Properties and Applications"' [viewed 2010 November 25]. Available from: http://www.sigmaaldrich.com/img/assets/15402/Detergent_Selection_Table.pdf.
17. Harshe R, Balan C, Riedel R. Amorphous Si(Al)OC ceramic from polysiloxanes: bulk ceramic processing, crystallization behavior and applications. *J Eur Ceram Soc* 2004;**24**:3471–82.
18. ASTM D 3576. Standard test method for cell size of rigid cellular plastics. *Annual book of ASTM standards*, vol. 08.02. West Conshohocken, PA: ASTM; 1997.
19. Li XH, Deng SD, Fu H, Mu GN. Inhibition action of tween-80 on the corrosion of cold rolled steel in sulfuric acid. *Mater Corros* 2009;**60**:969–76.
20. Wu J, Xu Y, Dabros T, Hamza H. Effect of EO and PO positions in non-ionic surfactants on surfactant properties and demulsification performance. *Colloids Surf A* 2005;**252**:79–85.
21. Fernandez P, Andre V, Rieger J, Kühnle A. Nano-emulsion formation by emulsion phase inversion. *Colloids Surf A* 2004;**251**:53–8.
22. Normatov J, Silverstein MS. Interconnected silsesquioxane-organic networks in porous nanocomposites synthesized within high internal phase emulsions. *Chem Mater* 2008;**20**:1571–7.
23. Colombo P, Bernardo E. Macro- and micro-cellular porous ceramics from preceramic polymers. *Compos Sci Technol* 2003;**63**:2353–9.
24. Gibson LJ, Ashby MF. *Cellular solids, structure and properties*. Cambridge, UK: Cambridge University Press; 1999.
25. Guo Z, Xiong J, Yang M, Xiong S, Chen J, Wu Y, et al. Dispersion of nano-TiN powder in aqueous media. *J Alloys Compd* 2010;**493**:362–7.
26. Ishihara S, Nishimura T, Tanaka H. Precipitation processing to synthesize fine polycarbosilane particles for precursors of silicon carbide powders. *J Ceram Soc Jpn* 2006;**114**:507–10.
27. Zhang Z, Feng S-S. In vitro investigation on poly(lactide) Tween 80 copolymer nanoparticles fabricated by dialysis method for chemotherapy. *Biomacromolecules* 2006;**7**:1139–46.
28. Wang A, Yin H, Ren M, Liu Y, Jiang T. Synergistic effect of silver seeds and organic modifiers on the morphology evolution mechanism of silver nanoparticles. *Appl Surf Sci* 2008;**254**:6527–36.
29. Brequel H, Parmentier J, Walter S, Badheka R, Trimmel G, Masse S, et al. Systematic structural characterization of the high-temperature behavior of nearly stoichiometric silicon oxycarbide glasses. *Chem Mater* 2004;**16**:2585–98.
30. Pena-Alonso R, Mariotto G, Gervais C, Babonneau F, Soraru GD. New insights on the high-temperature nanostructure evolution of SiOC and B-Doped SiBOC polymer-derived glasses. *Chem Mater* 2007;**19**:5694–702.
31. Ferrari AC, Robertson J. Interpretation of Raman spectra of disordered and amorphous carbon. *Phys Rev B: Condens Matter* 2000;**61**:14095.
32. Liang T, Li Y-L, Su D, Du H-B. Silicon oxycarbide ceramics with reduced carbon by pyrolysis of polysiloxanes in water vapor. *J Eur Ceram Soc* 2010;**30**:2677–82.
33. Mutin PH. Control of the composition and structure of silicon oxycarbide and oxynitride glasses derived from polysiloxane precursors. *J Sol–Gel Sci Technol* 1999;**14**:27–38.